Nat. Hazards Earth Syst. Sci. Discuss., 2, 3533–3559, 2014
www.nat-hazards-earth-syst-sci-discuss.net/2/3533/2014/
doi:10.5194/nhessd-2-3533-2014

Natural Hazards and Earth System Sciences
Open Access
Discussions

Anomalies of zenith tropospheric delay following the M_w 7.8 Haida Gwaii earthquake

Y. B. Yao[1,2], X. X. Lei[1], Q. Liu[1], C. Y. He[1], B. Zhang[1], and L. Zhang[1]

[1]School of Geodesy and Geomatics, Wuhan University, Wuhan 430079, China
[2]Key Laboratory of Geospace Environment and Geodesy, Ministry of Education, Wuhan University, Wuhan 430079, China

Received: 16 April 2014 – Accepted: 30 April 2014 – Published: 16 May 2014

Correspondence to: Y. B. Yao (ybyao@whu.edu.cn)

Published by Copernicus Publications on behalf of the European Geosciences Union.

Abstract

The 2012 Haida Gwaii earthquake was a massive M_w 7.8 earthquake that struck the Queen Carlotte Islands Region on 28 October 2012 (UTC). This study analyzed the variations in zenith tropospheric delay (ZTD) following the M_w 7.8 Haida Gwaii earthquake using near real-time ZTD data collected from eleven stations in the seismic region and the forecast ZTD of ECMWF. A new differential method was used to detect anomalies of ZTD time series. Result showed that obvious ZTD anomalies occurred on the day of the earthquake (day-of-year, doy 302). There were anomalous ZTD variations at eight stations in the post-earthquake period on doy 302, possibly due to the processes of earthquake-generated acoustic waves. Propagation of acoustic waves caused variations of tropospheric parameters (e.g., atmospheric pressure, temperate, and atmosphere density), thus influencing ZTD. Absence of anomalous ZTD variations at the remaining three stations was attributed to the special topographic conditions, i.e., the long epicentral distance and the presence of huge mountains as a natural protective screen. Our work provides new insights to the relationship between of earthquake event and ZTD variation. The proposed differential method is superior to conventional method for detecting specific ZTD anomalies caused by earthquake events.

1 Introduction

Earthquake is a calamitous natural disaster with huge destructive power. Large earthquakes commonly induce massive landslides and cause great losses to life and property. Earthquake research is thus of great significance (Calais et al., 1995; Yao et al., 2012a, b). A large number of investigations have found co-seismic or pre-seismic ionospheric anomalies and the speculated reason is the acoustic coupling of the atmosphere and the solid-Earth (Jin et al., 2011). During an earthquake, quick seismic surface wave propagation produces radiated sound and infrasonic waves, whose integrated interactions further generate locally ground-coupled air waves (Mikumo,

NHESSD
2, 3533–3559, 2014

1968). The air waves propagate first upward or obliquely toward the upper atmosphere and then spread horizontally as acoustic-gravity waves in the lower atmosphere (Mikumo, 2013). Numerous of studies have been investigated acoustic waves generated from earthquake sources, determined their velocity of propagation, and computed the seismic-to-pressure transfer function (e.g., Artru et al., 2004; Watada Set et al., 2006; Mikumo et al., 2008, 2013). The propagation of earthquake-generated acoustic waves in the troposphere may affect the global positioning system (GPS) signals and probably cause anomalous variations in zenith tropospheric delay (ZTD, Jin et al., 2011; Jin, 2012). However, recent studies lack of such possible impact on the troposphere and ZTD (Jin et al., 2011).

ZTD is an important parameter in the Global Navigation Satellite System (GNSS). Research on the internal mechanism of ZTD errors and their correlations with regional natural conditions are needed to find out accurate methods for correction of local atmospheric refraction errors (Yang, 2001). ZTD data can be obtained through GPS observations. By analyzing ZTD variations, Jin et al. (2011) firstly found that co-seismic tropospheric anomalies occurred during the main shock in lower atmosphere following the M_w 8.0 Wenchuan earthquake, and that daily ZTD residual time series (ZTD minus the daily mean) imply ZTD variations in the post-earthquake period. But the lower atmospheric anomalies, coupling processes and mechanism between the lower atmosphere and the solid-Earth with more cases and observation were unanswered.

Presently, investigations of more earthquake cases are required to promote the study of lower atmospheric anomalies and to understand the relationship between earthquake and ZTD (Jin et al., 2011). The present study aimed to detect short-term variations of ZTD following the M_w 7.8 Haida Gwaii earthquake that hit the Queen Carlotte Islands Region on 28 October 2012 (52.79° N, 132.1° W, 03:04:08, UTC) (IRIS). During the M_w 7.8 Haida Gwaii earthquake, seismogenic rupture surface of the shock extended northwestward and mainly southeastward, with a total length of approximately 100 km (Rosenberger et al., 2013). The main shock rupture was reported to spread at

NHESSD
2, 3533–3559, 2014

a rupture velocity of approximately 2.3 km s^{-1}, with an average slip of 3.3 m (Lay et al., 2013).

In this study, high-quality ZTD data were collected at eleven stations in the seismic region of Queen Carlotte Islands, and a new differential method was used for the first time to detect specific ZTD anomalies. Anomalous ZTD variations were analyzed at the eleven stations using high-precision troposphere products of zenith path delay (ZPD, another term for ZTD) provided by the International GNSS Service (IGS). To remove the zenith delay variations of usual change caused by weather changes as much as possible, we introduced the difference of the ZTD of IGS and the forecast data of ECMWF. Major conclusions were drawn and disturbances of ZTD were discussed based on a comprehensive analysis. The results will provide new insights to the relationship between of earthquake event and ZTD variation. The proposed differential method is superior to conventional method for detecting specific ZTD anomalies caused by earthquake events.

2 Data sources and analysis methods

ZTD is generated from the lower travel speed of GPS signals in the atmosphere than in vacuum, along a curved rather than straight path. It is essentially caused by the variations in atmospheric refractive index along the ray path (Bevis et al., 1992). Bevis et al. (1992) gave the excess path of the GPS signal as follows:

$$\Delta L = \int_L [n(s) - 1]\mathrm{d}s + [S - G] \quad (1)$$

where $n(s)$ is the refractive index; S is the path length along L; and G is the straight-line geometrical path length. The delay is mainly generated from the first part of Eq. (1) due to the slowing effect when the signals travel through the atmosphere (Bevis et al., 1992). In optics, the refractive index n of a substance is defined as $n = c/v$, where c

NHESSD
2, 3533–3559, 2014

is the speed of light in vacuum and v is the speed of light in the substance. In GNSS, this signal transmission delay is called tropospheric delay, which can be over 2 m at the zenith and 20 m at the lower elevation angles (Pena et al., 2001).

High-quality and near real-time ZTD products generated from GPS observations are supplied by IGS to meet the objectives of a wide range of scientific studies and engineering applications (Wang et al., 2007). At the IGS stations, ZPDs are estimated by the IGS Regional Network Associate Analysis Centers in support of the IGS Troposphere Working Group, which are available in subdirectories within the weekly GPS product directories (ftp://cddis.gsfc.nasa.gov/pub/gps/products/WWWW/trop; WWWW is the week number). These ZTDs are estimated by using GIPSY-OASIS software with IGS final combined orbit and clock products, IGS final combined earth orientation parameter, and site RINEX files (Wang et al., 2007). Other key features of the processing approach for IGS ZTD data are detailed by Byun and Bar-Sever (2009). In the present study, the accuracy of final ZTD products used was approximately 4 mm (Kouba, 2009). In addition, the forecast data of ZTD are supplied by the ECMWF.

This study was mainly focused on short-term ZTD changes during the M_w 7.8 Haida Gwaii earthquake, particularly in the post-earthquake period on the day of the earthquake (28 October 2012), i.e., day-of-year (doy) of 302. In view of the annual cycle of ZTD (Li et al., 2012), we analyzed ZTD data mainly on doy 299–305 in 2012 and doy 302 in 2000–2013. Additionally, ZTD data in October 2012 were studied at selected sites. Detailed information on the stations and parameters of GPS observation data are available in subdirectories of the IGS website (http://igscb.jpl.nasa.gov/index.html). The epicentral distance (distance between the epicenter and the station) of the observation sites ranged from approximately 370 km (station 1-HOLB) to 1200 km (station 11-PRDS). The increments of horizontal and vertical coordinates at these sites were small in the week studied (< 1 mm in most cases; maximum of approximately 1 cm at station 3-UCLU). Thus, effect on the accuracy of ZTD data posed by site displacement was neglected. According to local meteorological data (http://climate.weather.gc.ca), there was no abnormal weather on doy 302 in 2012. More information on the GPS

NHESSD
2, 3533–3559, 2014

sites (IGS stations) and earthquake parameters are shown in Fig. 1 and Tables 1 and 2.

ZTD variations were analyzed through multiple analysis using two important parameters, namely, mZTD (ZTD at each epoch minus the daily mean) and dZTD (ZTD at one epoch minus the prior epoch). First, a comparison analysis was performed on mZTD among the eleven stations. Then, a new differential method was used to analyze ZTD variations, demonstrating significant differences. Additionally, dZTD variations on doy 302 in 2012 were discussed. These increments indicated the ZTD variation trend in different dimensions. Based on statistical analysis of multi-year data, ZTD variations on doy 302 in 2012 were well demonstrated. Finally, the stations 6-ALBH and 9-WILL were taken as examples for statistical analysis of ZTD variations separately.

3 Data analysis

This study aimed to detect anomalous ZTD variations in the seismic region on doy 302 in 2012, and then to analyze their relationship with the earthquake event (if the anomalies exit). ZTD data at the IGS sites present a clear annual cycle and those at the medium- and high-latitude stations are given priority to the annual cycle (Li et al., 2012; Yao et al., 2013). According to the annual ZTD cycles and based on statistical analysis, we carried out multiple comparisons of data between doy 302 in 2012 and the other days (adjacent days in the same year and the same doy in different years). We analyzed ZTD variations at eleven stations in the seismic region to examine the difference in ZTD between doy 302 in 2012 and the other days. Detailed comparisons of ZTD were performed using mZTD, and a new method was used to better detect ZTD anomalies on doy 302 in 2012. Associated dZTD variations were also discussed.

NHESSD
2, 3533–3559, 2014

3.1 mZTD variations at eleven IGS stations

Sharp drop of ZTD clearly occurred at stations 1–8 on doy 302 in 2012 (Fig. 2). ZTD decreased by approximately dozens of millimeters at all of these sites and even reached 100 mm for a prolonged period at some stations (e.g., 1-HOLB and 6-ALBH); at the other stations, data were relatively smooth with the maximal ZTD variations mostly below 50 mm. For the maximal ZTD variation at station sites 1–8, the anomalies to some extent were related to the epicentral distance. Compared with data of doy 302 in 2012, ZTDs at station sites 1–8 were relative smooth on the other days. The geodetic azimuth between the epicenter and the sites was approximately the same at sites 3 and 4, with similar curves on doy 302 in 2012 (Table 2). The parallel tendency went for the sites 5 and 7 (Table 2).

At the remaining three station sites 9–11, there were no anomalous ZTD variations on doy 302 in 2012 compared with the other stations. This result indicated that the M_w 7.8 earthquake posed minor or no effects on ZTD at the three stations. Further analysis showed that several high mountains (the Rocky Mountains) were located between IGS stations 9–11 and the epicenter, while there were no such mountains or other visible blocks between stations 1–8 and the epicenter (Fig. 1). The epicenter of the M_w 7.8 earthquake was located in the Queen Carlotte Islands Region and cut off from the mainland by a long ridge (altitude 1000–2600 m) lying along the coastline and serving as a natural protective screen. Because stations 9–11 were located on the other side of the ridge, we speculated that the effects of massive earthquake on the station sites 9–11 were drastically or completely diminished in the presence of huge mountains. In fact, earthquake-originated infrasonic waves were sometimes converted into diffracted or reflected waves by the earth's surface topography during wave propagation in the atmosphere (Mikumo et al., 2010).

However, there still existed certain differences in the shape of ZTD curves on doy 302 in 2012 between individual stations. At station 1-HOLB, ZTD dramatically declined approximately 20–25 min after the earthquake and kept decreasing for 1 h, followed by

NHESSD
2, 3533–3559, 2014

a rebound to the original level (Fig. 2a). Considering that this station was nearest to the epicenter, its distinct difference of ZTD from the other stations might be related to the short epicentral distance. Similarly, stations 2–4 (NANO, UCLU, and BAMF) experienced rapid decreases in ZTD after the occurrence of earthquake. Another difference of the marked curves between individual stations lied in the variation trend hours after the earthquake that the sites 3-UCLU, 4-BAMF, and 6-ALBH showed another "protuberance" (Fig. 2c, d and f). We also noted that an obvious peak emerged on the ZTD curve of site 5-WSLR and 6-ALBH (Fig. 2e and h) with a trough before the huge earth shock. In short, this set of data implied that anomalous ZTD variations occurred at stations 1–8, and that the ZTD change rate on doy 302 in 2012 was related to the azimuth and the epicentral distance. The azimuth data were consistent with the strike of the fault plane at stations 1–8 but not at stations 9–11 (Tables 1 and 2).

Therefore, different ZTD variations of the two groups of stations (1–8 vs. 9–11) were attributed to earthquake-generated acoustic wave propagation. We speculated that when acoustic waves propagated in the troposphere under specific conditions, the acoustic waves generated by seismic waves might "break" smooth ZTD variations. This is despite that anomalous ZTD variations before the earthquake at sites 7 and 8 (Fig. 2g and h) might be derived from the propagation of "bubbles" generated from the underground fault (Molchanov et al., 2004). Together the above findings demonstrated that there were ZTD anomalies in the post-earthquake period on doy 302 in 2012, possibly induced by the occurrence of the earthquake.

3.2 ZTD anomalies detected by a new method

Because mZTD data only indicate rough variations in ZTD, a new method was used to detect ZTD anomalies by considering specific variations in ZTD. Due to rapid fluctuations of ZTD with occasionally high amplitude, ZTD anomalies are hard to be detected or observed sometimes. Because of the strong temporal correlation of ZTD, the proposed differential method removed the time influence on ZTD to a greater degree. The obtained results clearly showed the difference in ZTD variations between various days.

NHESSD
2, 3533–3559, 2014

ZTD time series is relatively smooth in normal circumstances but will turn distinct in the presence of anomalies. This feature helps to recognize the possible anomalies.

With the new detection method, we analyzed ZTD variation at station sites 1–8 in the seismic region. Results clearly showed that ZTD changed abnormally at sites 1-HOLB, 2-NANO, 4-BAMF, and 6-ALBH, with minor anomalies at sites 5-WSLR and 8-BREW and no anomalies at sites 10 and 11. After twice difference, most ZTD variations became relative smooth under normal conditions. At site 11-PRDS, ZTD changed normally on doy 302 as on the other days in 2012. Regarding annual ZTD cycle, sites 1–4 showed obvious anomalies (Fig. 3). In relation to local topography, sites 5-WSLR and 8-BREW (especially the latter site) might be affected by the mountains more or less, resulting in unclear or no ZTD anomalies.

To minimize the probability of anomalous ZTD changes all through the days adjacent to doy 302 in 2012, we examined ZTD at six sites on doy 300–304 in 2012. Similar to the situation on doy 302 in 2009–2013 (Fig. 3), ZTDs were distinct on doy 302 and generally normal on the other days in 2012 (doy 300–304, Fig. 4). Combined with the former set of data (Fig. 3), results obtained with the new differential method better distinguished the difference in ZTD and easily detected the anomalies between doy 302 and the adjacent days (doy 300–304) in 2012. We inferred that ZTD anomalies occurred on doy 302 in 2012 and were highly related to the occurrence of the earthquake. The earthquake effect on ZTD variations might be related to local topography and the epicentral distance to some extent. On the whole, the results obtained with the new differential method were consistent with data presented in Sect. 3.1. Details were obtained by using the new method and the results better reflected specific ZTD variations.

To gain information on ZTD variation rate, we analyzed dZTD at the eleven sites on doy 302 in 2012. Results show that dZTD fluctuated to varying degrees after the earthquake (Fig. 5), especially at sites 1–3 (Fig. 5a). Compared with the obvious fluctuations at sites 1–3 (Fig. 5a), the changes of dZTD at sites 4–11 (Fig. 5a, b and c) were relatively gentle in the post-earthquake period. This result showed that different effects of

NHESSD
2, 3533–3559, 2014

the earthquake might have lead to fluctuations of ZTD variation rate at sites 1–8 that were different from sites 9–11. As a result of these fluctuations, ZTDs as a whole were influenced.

3.3 Statistical significance of ZTD variations

3.3.1 Maximal ZTD variations at eleven stations on doy 302 in 2000–2013

As shown in Fig. 2, ZTD changed slowly within a day in most cases. If the maximal ZTD variation in a day was large, there could be a high probability of anomalies. In view of the annual ZTD cycle, we studied ZTD at the eleven IGS sites on doy 302 in 2000–2013 to minimize the influence of accidental factors. Results showed that the maximal ZTD variation at sites 1–8 on doy 302 were relatively large in 2012 compared with the other years (Fig. 6). The maximal ZTD variation showed statistically significant differences between doy 302 and the other days at sites 1–8 but not at sites 9–11. Similar significant differences were detected in mean maximal ZTD variation in the whole year of 2012. For example, mean maximal ZTD variation in 2012 was 45.41 mm at site 3-UCLU, while that on doy 302 was significantly greater, 86 mm. Considering the occurrence of the massive M_w 7.8 earthquake, we believed that the earthquake caused abnormal ZTD variations on doy 302 in 2012.

3.3.2 Maximal ZTD variations at eleven IGS stations in October 2012

Maximal ZTD variations in October 2012 were analyzed by multiple comparisons of data from sites 6-ALBH and 9-WILL. Results showed that the maximal ZTD variation on doy 302 in 2012 was statistically significant at site 6-ALBH but not at site 9-WILL. Similar results were observed at the other sites.

NHESSD
2, 3533–3559, 2014

3.4 Difference of the ZTD from IGS and the forecast data from ECMWF

To separate the zenith delay variations caused by the earthquake from usual change caused by weather changes as much as possible, we considered the forecast ZTD from the ECWMF (http://ggosatm.hg.tuwien.ac.at/DELAY/GRID/VMFG_FC/2012/), which can supply the best forecast ZTD currently. Troposphere mapping functions have been developed which are based on data from numerical weather models, e.g. from the European Centre for Medium-Range Weather Forecasts (ECMWF) (http://www.ecmwf.int). The Vienna Mapping Functions 1 (VMF1) from ECMWF are provided on a global grid ($2.5^{\circ} \times 2.0^{\circ}$), there are only four files per day, i.e. at 00:00, 06:00, 12:00, and 18:00 UT, and they are stored in yearly directories. We chose the nearest grid of ECMWF as the forecast data for each IGS station. Then based on the four files we could calculate the other time of the day with five minutes interval by interpolation. So the differences between the ZTD of IGS and the forecast data of ECMWF are available. Based on their differences, we can remove the usual change caused by the weather, so the differences change can be confirmed to be caused by other non-meteorological factors. In Fig. 8, the differences of doy 302 significantly decrease after the earthquake in the first four figures, while the last four figures have not so such clear changes. In short, Fig. 8 indicates that the M_w 7.8 earthquake is very likely to have caused the anomalies of ZTD.

3.5 Summary

The above results indicated that abnormal ZTD variations occurred during the post-earthquake period on doy 302 in 2012, which were likely caused by the earthquake event. The occurrence of earthquake affected ZTD variations at station sites 1–8 to varying degrees, especially within 10 h after the earthquake event. Significance of the earthquake effect was possibly related to factors such as the epicentral distance and the local topography.

NHESSD
2, 3533–3559, 2014

As shown in Eq. (1), ZTD is derived from variations in the tropospheric refractive index in nature. The delay is mainly generated from the first part in Eq. (1) and is caused by the slowing effect (Bevis et al., 1992). Variations in the tropospheric refractive index of GPS signals are due to changes in atmospheric temperature, pressure, and composition (Owens, 1967; Thayer, 1974; Pacione et al., 2003). Lighthill (1978) proposed the relationship between the pressure perturbation p_0, the air density ρ_0, sound velocity c_0 near the ground surface, and the vertical velocity of the ground as follows: $p_0 = \rho_0 c_0 w_0$. With recent deployment of the observation networks, a large number of observations have been reported on different types of earthquake-generated atmospheric waves, such as those from the 1968 Alaskan earthquake ($M_w \sim 9.0$) and the 2004 Sumatra-Andaman earthquake (Mikumo, 1968; Mikumo et al., 2009 etc.). These include high-frequency acoustic waves governed primarily by compressional force (Mikumo et al., 2009), which propagate in the lower atmosphere as well as up to the upper atmosphere (Garcés et al., 2009). In fact, the sudden vertical movement of the ground can excite atmospheric pressure perturbations with different frequencies (Mikumo, 1968; Watada et al., 2006; Mikumo et al., 2009). Additionally, some earthquake-generated acoustic waves strongly influence atmospheric temperature and air density (Kshevetskii et al., 2005; Tronin et al., 2004), and the transport of both momentum and energy are accompanied by the process of acoustic waves (Yeh et al., 1974).

4 Conclusions

This study conducted multiple comparisons of mZTD and dZTD using ZTD data from eleven IGS stations in the seismic region of the M_w 7.8 Haida Gwaii earthquake and the forecast ZTD data of ECMWF. Application of a new differential method enabled the detection of specific anomalies of ZTD time series and elimination of possible disturbances from local meteorology and IGS station displacement. Statistical data showed that there were significant differences in the maximal ZTD variation between doy 302 and the other days in 2012. The difference of the ZTD of IGS and the forecast data of

NHESSD
2, 3533–3559, 2014

ECMWF was also introduced. Together our findings implied that in the post-earthquake period on doy 302 in 2012, ZTD anomalies occurred to varying degrees at eight stations (1–8, especially 1–6) in the seismic region, possibly induced by the M_w 7.8 earthquake.

Regarding the mechanism through which the earthquake event influenced ZTD variations, we give the following explanation: acoustic waves generated from the M_w 7.8 Haida Gwaii earthquake caused anomalous ZTD variations in the troposphere (e.g., atmosphere pressure, temperate, atmosphere density), whereas the anomalies or their mutual effect led to variations in the atmospheric refractive index. Finally, the originated acoustic waves caused ZTD anomalies. During propagation in the atmosphere, some high-frequency acoustic waves originated from the M_w 7.8 earthquake source might have diffracted or reflected by the high mountain ridge lying along the coast line (Mikumo et al., 2010). Hence, there were three stations showing no anomalous ZTD variations as observed in the other eight stations. As to the anomalous ZTD variations in the delayed post-earthquake period (Fig. 2b–d), a possible explanation is that some high-frequency waves were probably bounced back from the earth surface and then transmitted by multiple refraction process to long distances, thereby influencing the ZTD again (Mutschlecner et al., 2005; Mikumo et al., 2010).

5 Discussion

We first estimated ZTD variations at the same epoch between the adjacent dates (days), namely, ZTD at one epoch on the current day minus the previous day. Since ZTD variations were greatly different in different dates, the above method failed to obtain ZTD anomalies effectively. We then examined the atmosphere pressure at the IGS station site BAMF, where the variation in atmospheric pressure on the day of the earthquake showed a gently rising trend while the variation on the other days mostly showed a moderately declining trend. The varying degrees of ZTD anomalies may be related to the epicentral distance and the local terrain. This effect on ZTD posed by the earthquake might be relevant to multiple parameters such as the strike of the fault plane,

NHESSD
2, 3533–3559, 2014

earthquake magnitude, and elevation of the site. More earthquake cases need to be analyzed to identify the possible and determinant factors.

However, the propagation of GPS signals is influenced by various near-surface factors in the troposphere, and the structure of atmospheric refractivity is highly complex and difficult to be described (Solheim et al., 1999). Lacks of sufficient earthquake cases and high temporal resolution observations are the major limitation of our study. Our work represents a preliminary work and more research in the future is essential. Determining the speed of acoustic wave propagation will be our next step of research.

In spite of the limitation, this study suggested that the occurrence of earthquake caused lower atmospheric anomalies (especially ZTD variations). We provided a possible explanation for the observed phenomenon and also introduced a new valid differential method to detect ZTD anomalies. The use of massive statistical data and the consideration of annual ZTD cycle were also the advantages of this study. Our work helps to improve the understanding of earthquake shock, ZTD, and their mutual relationship. More researches using data with high temporal resolution and more investigations for other earthquakes are needed to consolidate our conclusion and to thoroughly explain the coupling process between the solid-earth and the troposphere as well as their physical mechanisms.

Acknowledgements. The authors would like to thank the IGS, IRIS and ECMWF in their whole communities for providing ZTD data, earthquake information and the forecast ZTD data, respectively. This research was supported by the National High Technology Research and Development Program of China (2013AA122502) and the National Natural Science Foundation of China (41174012; 41274022) and the Fundamental Research Funds for the Central Universities.

References

Arai, N., Iwakuni, M., Watada, S. et al.: Atmospheric boundary waves excited by the tsunami generation related to the 2011 great Tohoku-Oki earthquake, Geophys. Res. Lett., 38, L00G18, doi:10.1029/2011GL049146, 2011.

NHESSD
2, 3533–3559, 2014

Artru, J., Farges, T., and Lognonné, P.: Acoustic waves generated from seismic surface waves: propagation properties determined from Doppler sounding observations and normal-mode modelling, Geophys. J. Int., 158, 1067–1077, 2004.
Barry, R. G. and Chorley, R. J.: Atmosphere, Weather and Climate, Psychology Press, 2003.
Bevis, M., Businger, S., Herring, T. A. et al.: GPS meteorology: remote sensing of atmospheric water vapor using the Global Positioning System, J. Geophys. Res.-Atmos., 97, 15787–15801, 1992.
Byun, S. H. and Bar-Sever, Y. E.: A new type of troposphere zenith path delay product of the international GNSS service, J. Geodesy, 83, 1–7, 2009.
Calais, E. and Minster, J. B.: GPS detection of ionospheric perturbations following the January 17, 1994, Northridge earthquake, Geophys. Res. Lett., 22, 1045–1048, 1995.
Garcés, M., Willis, M., and Le Pichon, A.: Infrasonic observations of open ocean swells in the Pacific: deciphering the song of the sea, in: Infrasound Monitoring for Atmospheric Studies, Springer, Netherlands, 235–248, 2009.
Jin, S.: GNSS atmospheric seismology: a case study of the 2008 M_w 7.9 Wenchuan earthquake, Geoscience and Remote Sensing Symposium (IGARSS), 2012 IEEE International, 7504–7507, 2012.
Jin, S., Han, L., and Cho, J.: Lower atmospheric anomalies following the 2008 Wenchuan Earthquake observed by GPS measurements, J. Atmos. Sol.-Terr. Phy., 73, 810–814, 2011.
Kouba, J.: A guide to using International GNSS Service (IGS) products, available at: http://igscb.jpl.nasa.gov/igscb/resource/pubs/UsingIGSProductsVer21.pdf, 2009.
Kshevetskii, S. P. and Gavrilov, N. M.: Vertical propagation, breaking and effects of nonlinear gravity waves in the atmosphere, J. Atmos. Sol.-Terr. Phy., 67, 1014–1030, 2005.
Lay, T., Ye, L., Kanamori, H. et al.: The October 28, 2012 M_w 7.8 Haida Gwaii underthrusting earthquake and tsunami: slip partitioning along the Queen Charlotte Fault transpressional plate boundary, Earth Planet. Sc. Lett., 375, 57–70, 2013.
Lighthill, J.: Waves in Fluids, Cambridge University Press, New York, 1978.
Li, W., Yuan, Y. B., Ou, J. K. et al.: A new global zenith tropospheric delay model IGGtrop for GNSS applications, Chinese Sci. Bull., 57, 2132–2139, 2012.
Mikumo, T.: Atmospheric pressure waves and tectonic deformation associated with the Alaskan earthquake of March 28, 1964, J. Geophys. Res., 73, 2009–2025, 1968.
Mikumo, T. and Watada, S.: Acoustic-gravity waves from earthquake sources, in: Infrasound Monitoring for Atmospheric Studies, Springer, Netherlands, 263–279, 2009.

NHESSD
2, 3533–3559, 2014

Mikumo, T., Shibutani, T., Le Pichon, A. et al.: Low-frequency acoustic-gravity waves from coseismic vertical deformation associated with the 2004 Sumatra-Andaman earthquake (M_w = 9.2), J. Geophys. Res., 113, B12402, doi:10.1029/2008JB005710, 2008.

Mikumo, T., Garces, M., Shibutani, T. et al.: Acoustic-gravity waves from the source region of the 2011 great Tohoku earthquake (M_w = 9.0), J. Geophys. Res.-Sol. Ea., 118, 1534–1545, 2013.

Molchanov, O., Fedorov, E., Schekotov, A., Gordeev, E., Chebrov, V., Surkov, V., Rozhnoi, A., Andreevsky, S., Iudin, D., Yunga, S., Lutikov, A., Hayakawa, M., and Biagi, P. F.: Lithosphere–atmosphere–ionosphere coupling as governing mechanism for preseismic short-term events in atmosphere and ionosphere, Nat. Hazards Earth Syst. Sci., 4, 757–767, doi:10.5194/nhess-4-757-2004, 2004.

Mutschlecner, J. P. and Whitaker, R. W.: Infrasound from earthquakes, J. Geophys. Res.-Atmos., 110, D01108, doi:10.1029/2004JD005067, 2005.

Nappo, C. J.: An Introduction to Atmospheric Gravity Waves, Elsevier, 2012.

Niell, A. E.: Global mapping functions for the atmosphere delay at radio wavelengths, J. Geophys. Res., 101, 3227–3246, 1996.

Owens, J. C.: Optical refractive index of air: dependence on pressure, temperature and composition, Appl. Optics, 6, 51–59, 1967.

Pacione, R. and Vespe, F.: GPS zenith total delay estimation in the Mediterranean area for climatological and meteorological applications, J. Atmos. Ocean. Tech., 20, 1034–1042, 2003.

Penna, N., Dodson, A. H., and Chen, W.: Assessment of EGNOS tropospheric correction model, J. Navigation, 54, 1401–1407, 2001.

Rosenberger, A., Bird, A., Turek, M. E. et al.: Strong Motion Data from the Magnitude 7.7 “Haida Gwaii” Earthquake on October 27, 2012 (local time), 2013.

Solheim, F. S., Vivekanandan, J., Ware, R. H. et al.: Propagation delays induced in GPS signals by dry air, water vapor, hydrometeors, and other particulates, J. Geophys. Res., 104, 9663–9670, 1999.

Struzak, R.: Radio-wave propagation basics, Saatavissa, available at: http://wireless.ictp.it/school_2006/lectures/Struzak/RadioPropBasics-ebook.pdf, Hakupäivä, 7, 2011, 2006.

Thayer, G. D.: An improved equation for the radio refractive index of air, Radio Sci., 9, 803–807, 1974.

NHESSD

2, 3533–3559, 2014

Tronin, A. A., Biagi, P. F., Molchanov, O. A. et al.: Temperature variations related to earthquakes from simultaneous observation at the ground stations and by satellites in Kamchatka area, Phys. Chem. Earth, 29, 501–506, 2004.

Wang, J., Zhang, L., Dai, A. et al.: A near-global, 2-hourly data set of atmospheric precipitable water from ground-based GPS measurements, J. Geophys. Res.-Atmos., 112, D11107, doi:10.1029/2006JD007529, 2007.

Watada, S., Kunugi, T., Hirata, K. et al.: Atmospheric pressure change associated with the 2003 Tokachi-Oki earthquake, Geophys. Res. Lett., 33, L24306, doi:10.1029/2006GL027967, 2006.

Yang, L.: The Theory and Research of Atmosphere affection to GPS Surveying, The PLA Institute of Surveying and Mapping, Information Engineering University, Zhengzhou, 2001.

Yao, Y. B., Chen, P., Zhang, S., Chen, J. J., Yan, F., and Peng, W. F.: Analysis of pre-earthquake ionospheric anomalies before the global M = 7.0+ earthquakes in 2010, Nat. Hazards Earth Syst. Sci., 12, 575–585, doi:10.5194/nhess-12-575-2012, 2012a.

Yao, Y. B., Chen, P., Wu, H. et al.: Analysis of ionospheric anomalies before the 2011 M_w 9.0 Japan earthquake, Chinese Sci. Bull., 57, 355–365, 2012b.

Yao, Y. B., He, C. Y., Zhang, B. et al.: A new global zenith tropospheric delay model GZTD, Chinese J. Geophys.-Ch., 56, 2218–2227, 2013.

Yeh, K. C. and Liu, C. H.: Acoustic-gravity waves in the upper atmosphere, Rev. Geophys., 12, 193–216, 1974.

NHESSD

2, 3533–3559, 2014

Table 1. Parameters of the M_w 7.8 Haida Gwaii earthquake (http://www.iris.edu, Lay et al., 2013).

Mag	Date	Day of year	Time (UTC)	Latitude (° N)	Longitude (° W)	Depth (km)	Strike (°)	Height (m)
7.8	28 Oct 2012	302	03:04:08.8	52.79	132.1	14	317.7	6

NHESSD
2, 3533–3559, 2014

Table 2. Locations of eleven IGS stations (http://igscb.jpl.nasa.gov/network/network.php).

No.	Stations ID	Latitude (° N)	Longitude (° W)	Azimuth (°)	Distance (km)
1	HOLB	50.64	128.14	126.5	358
2	NANO	49.30	124.09	117.2	657
3	UCLU	48.93	125.54	128.5	670
4	BAMF	48.84	125.14	128.5	670
5	WSLR	50.13	122.92	103.4	735
6	ALBH	48.39	123.49	121	782
7	DRAO	49.32	119.63	104.5	979
8	BREW	48.13	119.68	110.3	1030
9	WILL	52.24	122.17	86	686
10	WHIT	60.75	135.22	349.2	909
11	PRDS	50.87	114.30	92.5	1279

Azimuth is the geodetic azimuth between the epicenter and the site.

NHESSD
2, 3533–3559, 2014

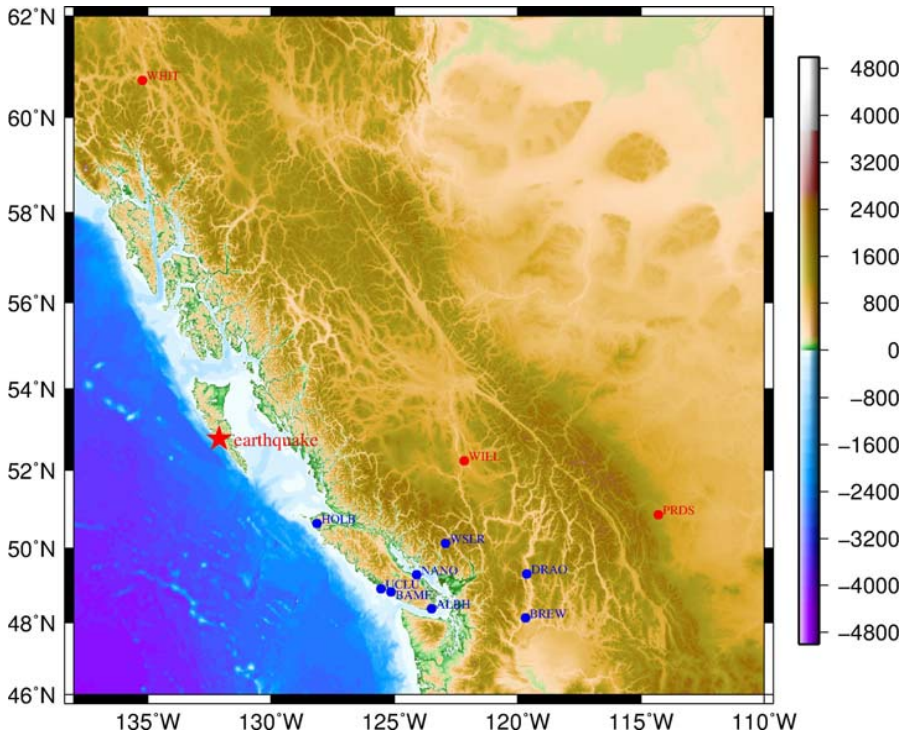

Fig. 1. Distribution of eleven IGS stations in the seismic region of M_w 7.8 Haida Gwaii earthquake. Red star represents the epicenter; blue dots represent the stations at which anomalous variations of ZTD were observed; and red dots represent the stations at which anomalous variations of ZTD were not observed.

NHESSD
2, 3533–3559, 2014

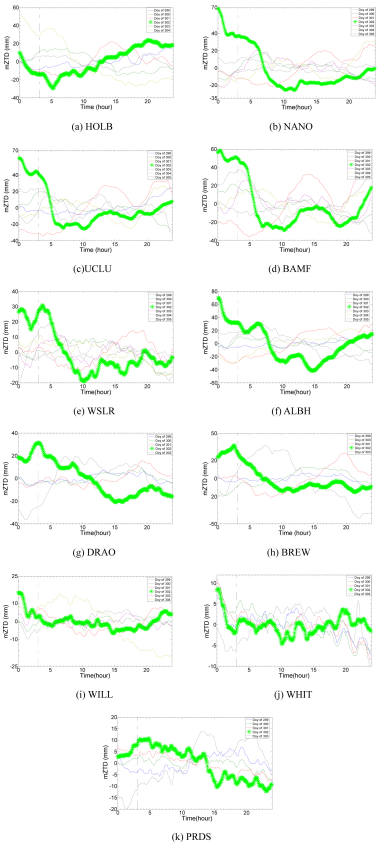

Fig. 2. Variations of mZTD at eleven IGS stations in the seismic region of M_w 7.8 Haida Gwaii earthquake. Marked curves represent ZTD variations on the day of the earthquake (doy 302, 2012); and dotted lines represent the epoch of the earthquake. Data cover 0:00 to 24:00 (UTC). ZTD estimations were missing at some sites for few days.

NHESSD
2, 3533–3559, 2014

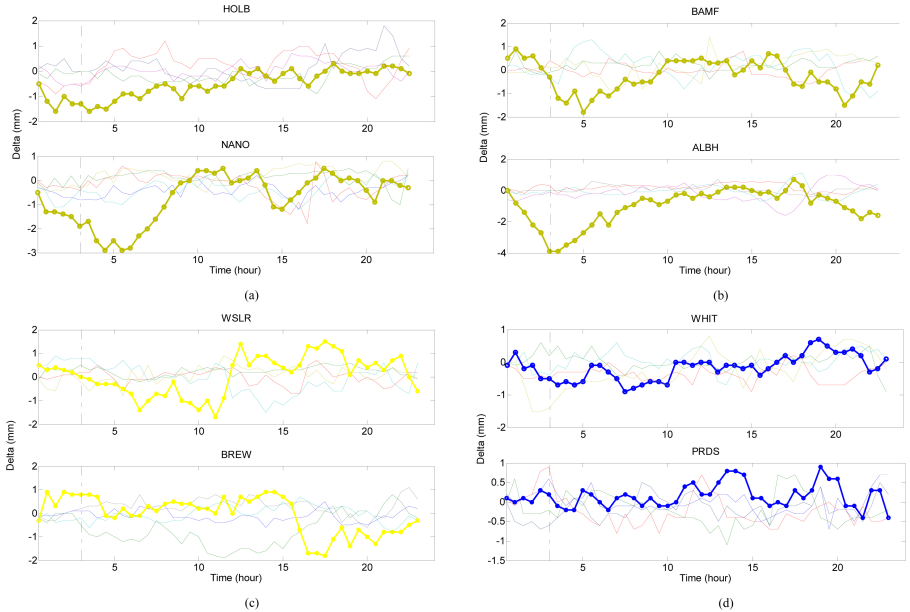

Fig. 3. Variation of ZTD after twice difference at eight IGS sites in the seismic region of M_w 7.8 Haida Gwaii earthquake on day-of-year (doy) 302 in 2009–2013. Time interval is half an hour. Marked curves represent ZTD variations on the day of the earthquake (doy 302, 2012), and other curves represent ZTD variations on the same doy in 2009–2011 and 2013. The dotted lines represent the epoch of the earthquake.

NHESSD
2, 3533–3559, 2014

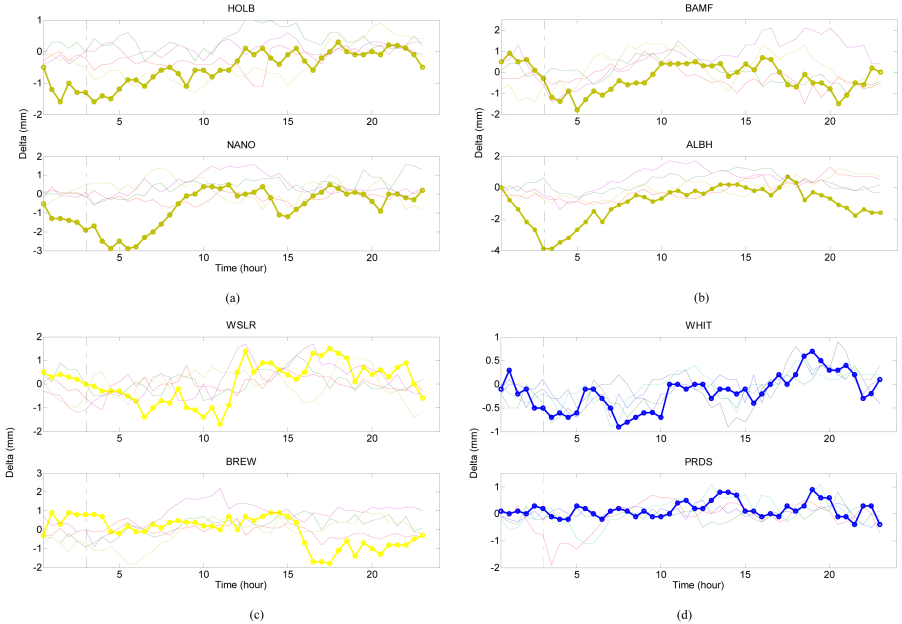

Fig. 4. Variation of ZTD after twice difference at eight IGS sites in the seismic region of M_w 7.8 Haida Gwaii earthquake on day-of-year (doy) 300–304 in 2012. Time interval is half an hour. Marked curves represent ZTD variations on the day of the earthquake (doy 302, 2012); other curves represent ZTD variations on doy 300, 301, 303, and 304; dotted lines represent the epoch of the earthquake. At site 10-WHIT, ZTD on doy 303 was missing and thus was substituted by ZTD on doy 305.

NHESSD
2, 3533–3559, 2014

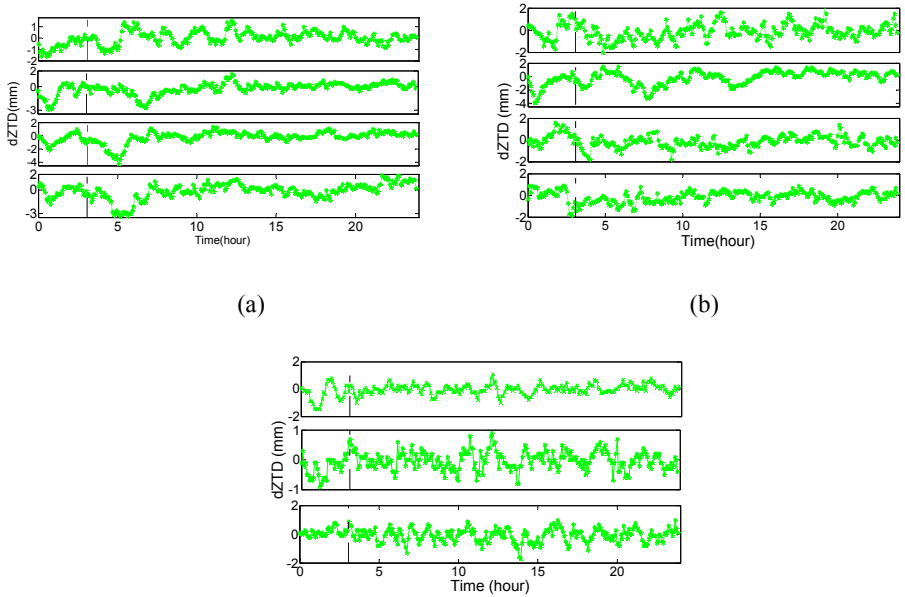

Fig. 5. Comparisons of dZTD variations at eleven IGS sites in the seismic region of M_w 7.8 Haida Gwaii earthquake on the day of the earthquake (day-of-year 302, 2012). **(a)** 1-HOLB, 2-NANO, 3-UCLU and 4-BAMF; **(b)** 5-WSLR, 6-ALBH, 7-DRAO and 8-BREW; and **(c)** 9-WILL, 10-WHIT and 11-PRDS. Dotted lines represent the epoch of the earthquake.

NHESSD
2, 3533–3559, 2014

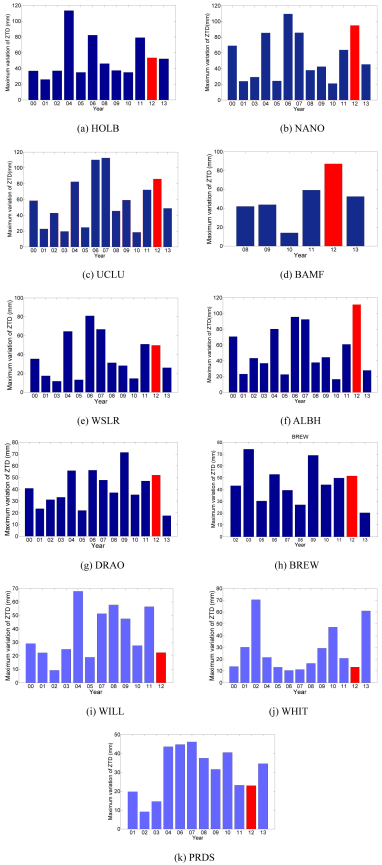

Fig. 6. Comparisons of the maximal ZTD variations at eleven IGS sites in the seismic region of M_w 7.8 Haida Gwaii earthquake on day-of-year (doy) 302 in 2000–2013. Red bars represent 2012. ZTD estimations were missing at some sites (especially BAMF) for few days.

NHESSD
2, 3533–3559, 2014

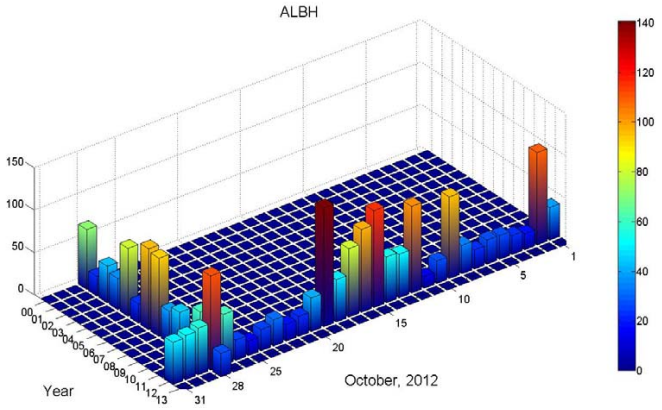

(a)

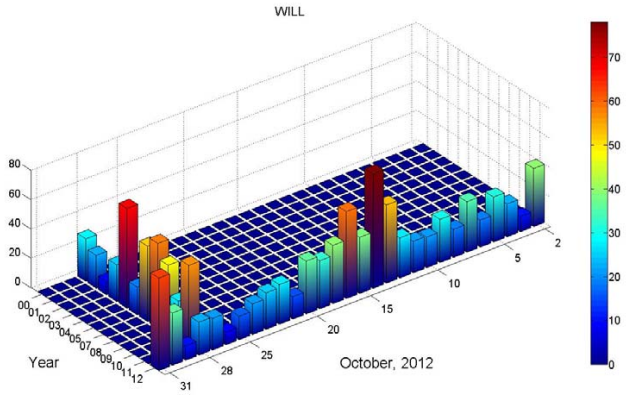

(b)

Fig. 7. Comparisons of the maximal ZTD variations at two IGS sites in the seismic region of M_w 7.8 Haida Gwaii earthquake in October 2012 and ZTD variations on day-of-year (doy) 302 in 2000–2013. **(a)** 6-ALBH; and **(b)** 9-WILL. Histogram bars are colored according to height.

NHESSD
2, 3533–3559, 2014

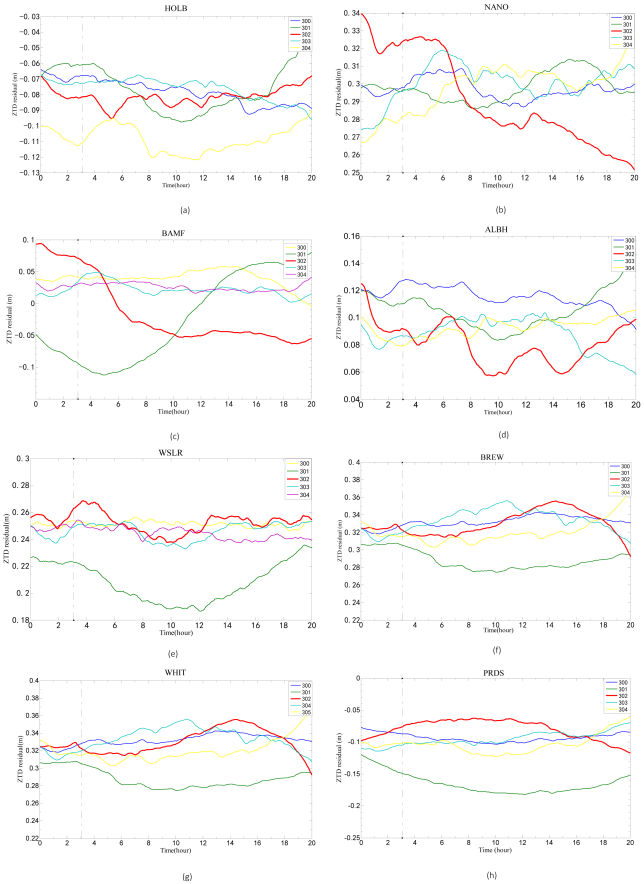

Fig. 8. Difference between the ZTD of IGS station and the forecast ZTD data of ECWMF on the day mainly from doy 300 to 304 in 2012. The dotted lines represent the epoch of the earthquake. At site 7-WHIT, ZTD on doy 303 was missing and thus was substituted by ZTD on doy 305.

NHESSD
2, 3533–3559, 2014